LOWLAND TECHNOLOGY INTERNATIONAL Vol. 3, No. 2, 58-73, December 2001
International Association of Lowland Technology (IALT), ISSN 1344-9656

TIME-DEPENDENT ELASTOPLASTIC CONSTITUTIVE EQUATION OF SOILS AND ITS APPLICATION TO FEM IMPLEMENTATION

T. Okayasu[1] and K. Hashiguchi[2]

ABSTRACT: The *time-dependent subloading surface model* (Hashiguchi and Okayasu 2000) would predict time-dependent elastoplastic deformation of materials pertinently. In this article the equation of the creep stretching formulated in the previous article for soils is extended so as to predict the time-dependent deformation of soils more accurately. Its adequacy is evaluated by comparisons with test data under undrained triaxial compression. Further, the finite element method (FEM) program for the prediction of time-dependent elastoplastic deformation behavior of soil structures is developed based on the time-dependent subloading surface model, the soil-water coupled formulation and the finite deformation theory. The ability of the FEM program is examined for the simulation of one-dimensional consolidation phenomenon.

INTRODUCTION

In clayey soft grounds, irreversible large deformation is caused by construction of soil structures such as embankments, tunnels, excavations and so on. Further, the deformation that is called the *secondary consolidation* or the *secondary consolidation effect* is continuously observed for very long term after the completion of construction.

Various constitutive models for describing time-dependent behavior of soils have been proposed up to the present. They could be classified into three kinds of approaches, i.e. the *over-stress model* (Adachi and Okano 1974; Adachi and Oka 1982; Liang and Ma 1992) originated by Perzyna (1963a, b, 1966), the *nonstationary flow surface model* (Sekiguchi 1977, 1984; Sekiguchi and Ohta 1977; Nova 1982; Matsui and Abe 1985) originated by Olzak and Perzyna (1966, 1970) and the *superposition model* (Dafalias 1982; Kaliakin and Dafalias 1990a, b; Tian et al. 1994; Al-Shamrani and Sture 1998). However, these models could not be applicable to the description of deformation behavior for a wide range of stress below and over the elastic limit as was analyzed by Hashiguchi and Okayasu (2000) in detail.

Plastic deformation due to the mutual slip between microstructures is suppressed under a high-rate deformation causing the increase of viscous resistance acting between microstructures of the materials, e.g. crystals or polycrystals for metals and soil particles for soils. Therefore, when a large deformation is induced at a high rate, the stress would go out the yield surface since the deformation proceeds elastically, whilst the plastic deformation is suppressed by the viscous resistance and thus the yield surface is almost fixed. The *subloading surface model* (Hashiguchi and Ueno 1977; Hashiguchi 1980, 1989; Hashiguchi and Chen 1998) does not premise that the stress exists on the *normal-yield surface* (conventional yield surface) even in the plastic loading process. In this model the *subloading surface* is introduced, which passes always through the stress point even when the stress exists inside the normal-yield surface and is similar to the normal-yield surface, and it is

1 Science Researcher, Department of Agricultural Engineering, Kyushu University, Fukuoka 812-8581, JAPAN.
2 Professor, ditto.
Note: Discussion on this paper is open until June 1, 2002.

assumed that the subloading surface approaches to the normal-yield surface in the plastic loading process. Hashiguchi and Okayasu (2000) extended this model so as to describe the time-dependent deformation behavior by allowing the subloading surface to become larger than the normal-yield surface and introducing the creep stretching which proceeds with time and further proposed the constitutive equation for soils by incorporating the secondary-consolidation phenomenon. Its adequacy has been also verified by comparing it with experimental data on fundamental time-dependent behavior under undrained condition.

In this article the creep stretching of the model is extended so as to predict the time-dependent deformation of soils more accurately. The adequacy is evaluated by comparisons with test data under the undrained triaxial compression. Further, the finite element method (FEM) program for the prediction of the time-dependent elastoplastic deformation behavior of soil structures is developed based on the time-dependent subloading surface model, the soil-water coupled formulation (Akai and Tamura 1978) and the finite deformation theory (Yatomi et al 1989). The capability of the FEM program is examined for the simulation of one-dimensional consolidation phenomenon.

The signs of a stress (rate) and a stretching (a symmetric part of velocity gradient) components are taken to be positive for tension, and the stress for soils is meant to be the *effective stress*, i. e. the stress excluded a pore pressure from the total stress throughout this article.

THE TIME-DEPENDENT SUBLOADING SURFACE MODEL

In this section the outline of the time-dependent subloading surface model is explained since it is essential for development of the FEM program.

Let it be assumed that the stretching $\mathbf{D}$ is additively decomposed into the elastic stretching $\mathbf{D}^e$ due to deformation of solid particles and the inelastic stretching $\mathbf{D}^{pc}$, called the *plastic-creep stretching*, due to mutual slip between solid particles:

$$\mathbf{D} = \mathbf{D}^e + \mathbf{D}^{pc} \tag{1}$$

where the elastic stretching $\mathbf{D}^e$ is given by

$$\mathbf{D}^e = \mathbf{E}^{-1}\overset{\circ}{\mathbf{T}} \tag{2}$$

$\mathbf{T}$ is a stress, $(^\circ)$ indicates the proper corotational rate with the objectivity (cf. e.g. Dafalias 1985; Zbib and Aifantis 1988) and the fourth-order tensor $\mathbf{E}$ is the elastic modulus given in the Hooke's type as

$$E_{ijkl} = (K - \frac{2}{3}G)\delta_{ij}\delta_{kl} + G(\delta_{ik}\delta_{jl} + \delta_{il}\delta_{jk}) \tag{3}$$

where K and G are the bulk and the shear modulus, respectively, which are functions of stress and internal state variables in general and δ_{ij} is the Kronecker's delta, i.e. $\delta_{ij} = 1$ for $i = j$ and $\delta_{ij} = 0$ for $i \neq j$.

Let it be assumed that the plastic-creep stretching $\mathbf{D}^{pc}$ is further additively decomposed into the plastic stretching $\mathbf{D}^p$ induced by the stress rate and the *creep stretching* $\mathbf{D}^c$ always induced by the elapse of time without a loading criterion, i.e.

$$\mathbf{D}^{pc} = \mathbf{D}^{p} + \mathbf{D}^{c} \tag{4}$$

Normal-Yield and Subloading Surfaces

Assume the yield condition:

$$f(\mathbb{S}) = F(H) \tag{5}$$

where the scalar H is the isotropic hardening/softening variable. Let it be assumed that the function f is homogeneous of degree one in the stress tensor $\mathbb{S}$. Then, the yield surface keeps a similar shape. Hereinafter, let the elastoplastic constitutive equation be formulated in the framework of the *unconventional plasticity* defined by DRUCKER (1988) as the extended plasticity such that the interior of yield surface is not a purely elastic domain but plastic deformation is induced by the rate of stress inside the yield surface. Thus, the conventional yield surface is renamed as the *normal-yield surface* in the present model.

Now, let the *subloading surface* (Hashiguchi and Ueno 1977; Hashiguchi 1980, 1989) be introduced, which always passes through the current stress $\mathbb{S}$ and keeps the similarity to the normal-yield surface with respect to the origin of stress space, i.e. $\mathbb{S} = \mathbf{0}$. Besides, the ratio of the size of the subloading surface to that of the normal-yield surface is denoted by R which can be regarded also as the measure of approaching degree to the normal-yield state and thus is called the *normal-yield ratio*. The conjugate stress $\mathbb{S}_y$ on the normal-yield surface for the current stress $\mathbb{S}$ on the subloading surface due to the similarity is given by

$$\mathbb{S}_y = \frac{\mathbb{S}}{R} \tag{6}$$

By substituting Eq. (6) into Eq. (5) with regarding $\mathbb{S}$ in Eq. (5) as $\mathbb{S}_y$, the subloading surface is described as

$$f(\mathbb{S}) = RF(H) \tag{7}$$

The normal-yield and the subloading surfaces are depicted in Fig. 1.

The time-differentiation of Eq. (7) for the subloading surface is given by

$$\mathrm{tr}\left(\frac{\partial f(\mathbb{S})}{\partial \mathbb{S}}\overset{\circ}{\mathbb{S}}\right) = \dot{R}F + RF'\dot{H} \tag{8}$$

where

$$F' \equiv \frac{dF}{dH} \tag{9}$$

tr( ) denotes the trace and $(\overset{\circ}{\ })$ stands for the material-time derivative. Further, it can be interpreted that the internal structure of materials changes not only with the plastic stretching but also with the creep stretching. Then, taking account of the plastic-creep stretching decomposition defined in Eq. (4) and the fact that the mutual slip of solid particles and the alteration of slip-characteristics is caused by the creep stretching as well as the plastic stretching, let it be assumed that an internal variable is additively decomposed into the plastic

and the creep part. Hence, the evolution rule of the isotropic hardening/softening variable H is extended as

$$\dot{H} = \dot{H}^p + \dot{H}^c \tag{10}$$

where $\dot{H}^p$ and $\dot{H}^c$ are the same functions f_H of $\mathbf{D}^p$ and $\mathbf{D}^c$, respectively, in homogenous degree one as follows:

$$\dot{H}^p = f_H(\mathbb{S}, \mathbf{D}^p), \quad \dot{H}^c = f_H(\mathbb{S}, \mathbf{D}^c) \tag{11}$$

Let the evolution equation of the normal-yield ratio R be given by

$$\dot{R} = U^t \left\| \mathbf{D}^p \right\| \text{ for } \mathbf{D}^p \neq \mathbf{0} \tag{12}$$

where U^t is the function of R and $\|\mathbf{D}\|$, which monotonically decreases with R and increases with $\|\mathbf{D}\|$ satisfying

$$\left.\begin{aligned} U^t &= U_R \quad \text{for } \|\mathbf{D}\| = 0, \\ U^t &> U_R \quad \text{for } \|\mathbf{D}\| > 0, \end{aligned}\right\} \tag{13}$$

and thus it results that $\dot{R} > 0$ even in $R = 1$ if $\|\mathbf{D}\| > 0$. The function U^t is illustrated in Fig. 2. The concrete form of the function U^t is given additively as

$$U^t = U_R(R) + U_D(\|\mathbf{D}\|) \tag{14}$$

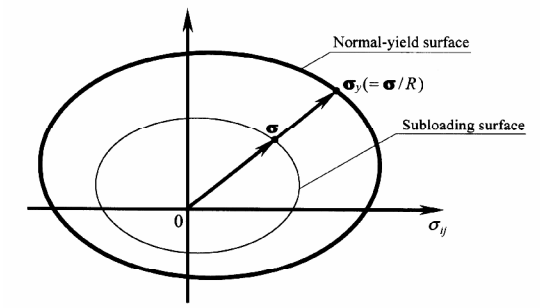

Fig. 1 Normal-yield and subloading surfaces Plastic Stretching

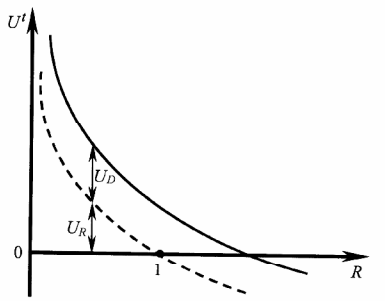

Fig. 2 Function U^t in the evolution rule of the normal-yield ratio R

where U_D (≥ 0) is the monotonically increasing function of $\|\mathbf{D}\|$, satisfying

$$U_D = 0 \quad \text{for } \|\mathbf{D}\| = 0 \tag{15}$$

The simplest function U_D satisfying Eq. (15) is given by

$$U_D = \zeta \|\mathbf{D}\| \tag{16}$$

where ζ is the material constant.

In this extended model the normal-yield ratio R is regarded as a measure describing the degree that a stress approaches to the normal-yield surface or goes out it, whilst the stress goes out the normal-yield surface, resulting in $R > 1$, at a high rate of deformation.

The consistency condition extended for time-dependent deformation is given from Eq. (8) with Eqs. (10) and (12) as

$$\mathrm{tr}\left(\frac{\partial f(\boldsymbol{\sigma})}{\partial \boldsymbol{\sigma}} \overset{\circ}{\boldsymbol{\sigma}}\right) = U^t \|\mathbf{D}^p\| F + RF'(\dot{H}^p + \dot{H}^c) \tag{17}$$

Assume the associated flow rule for the subloading surface

$$\mathbf{D}^p = \lambda \mathbf{N} \quad \left(\mathbf{N} \equiv \frac{\partial f(\boldsymbol{\sigma})}{\partial \boldsymbol{\sigma}} \Big/ \left\| \frac{\partial f(\boldsymbol{\sigma})}{\partial \boldsymbol{\sigma}} \right\|\right) \tag{18}$$

where λ (>0) is the proportionality factor and the second-order tensor $\mathbf{N}$ is the normalized outward-normal of the subloading surface.

The substitution of Eq. (18) into the extended consistency condition (17) leads to

$$\lambda = \frac{\mathrm{tr}(\mathbf{N}\overset{\circ}{\boldsymbol{\sigma}}) - \dfrac{F'}{F}\dot{H}^c \,\mathrm{tr}(\mathbf{N}\boldsymbol{\sigma})}{M_p^t} \tag{19}$$

where

$$M_p^t \equiv \left(\frac{F'}{F} h^p + \frac{U^t}{R}\right) \mathrm{tr}(\mathbf{N}\boldsymbol{\sigma}) \tag{20}$$

$$h^p \equiv \frac{\dot{H}^p}{\lambda} \tag{21}$$

It should be noted that the plastic modulus M_p^t becomes larger and thus the magnitude of plastic stretching becomes smaller at a higher rate of deformation since M_p^t is the monotonically increasing function of the magnitude of stretching $\|\mathbf{D}\|$ through the extended function U^t in Eq. (14).

Noting that the internal variable describing the alteration of the creep deformation would be also influenced by the plastic deformation as well as the creep deformation, let the creep stretching $\mathbf{D}^c$ be given as

$$\mathbf{D}^c = \mathbf{T}(\boldsymbol{\sigma}, H) \tag{22}$$

where $\mathbf{T}$ is the second-order tensor function of the stress $\boldsymbol{\sigma}$ and the internal state variable H in general.

It holds from Eqs. (1), (2), (4), (8), (18), (19) and (22) that

$$\mathbf{D}=\mathbf{E}^{-1}\overset{\circ}{\boldsymbol{\sigma}}+\frac{\mathrm{tr}(\mathbf{N}\overset{\circ}{\boldsymbol{\sigma}})-\frac{F'}{F}\dot{H}^{c}\,\mathrm{tr}(\mathbf{N}\boldsymbol{\sigma})}{M_{p}^{t}}\mathbf{N}+\mathbf{T} \tag{23}$$

The positive proportionality factor λ, rewritten as Λ, is described in terms of the stretching $\boldsymbol{D}$ from Eq. (23) as

$$\Lambda=\frac{\mathrm{tr}(\mathbf{NED})-\frac{F'}{F}\dot{H}^{c}\,\mathrm{tr}(\mathbf{N}\boldsymbol{\sigma})-\mathrm{tr}(\mathbf{NET})}{M_{p}^{t}+\mathrm{tr}(\mathbf{NEN})} \tag{24}$$

The stress rate is given from Eqs. (1), (2), (4), (8), (18), (19), (22) and (24) as

$$\overset{\circ}{\boldsymbol{\sigma}}=\mathbf{ED}-\frac{\mathrm{tr}(\mathbf{NED})-\frac{F'}{F}\dot{H}^{c}\,\mathrm{tr}(\mathbf{N}\boldsymbol{\sigma})-\mathrm{tr}(\mathbf{NET})}{M_{p}^{t}+\mathrm{tr}(\mathbf{NEN})}\mathbf{EN}-\mathbf{ET} \tag{25}$$

Note that the stretching $\mathbf{D}$ cannot be expressed analytically in terms of the stress rate $\overset{\circ}{\boldsymbol{\sigma}}$ since the right-hand side of Eq. (23) includes $\mathbf{D}$ but inversely the stress rate $\overset{\circ}{\boldsymbol{\sigma}}$ is expressed analytically in terms of the stretching $\mathbf{D}$ as seen in Eq. (25). Besides, the constitutive equation (23) or (25) is of the so-called *rate-nonlinearity* since it includes the magnitude of stretching $\|\mathbf{D}\|$. The rate-nonlinearly is the inevitable property of rate-type constitutive equations for describing the time-dependent behavior since the stiffness modulus relating the stress rate to the stretching has to depend on the rate variable, i.e. the stretching or the stress rate.

A loading criterion would not be necessary for the creep stretching since it proceeds always with the elapse of time. On the other hand, taking the fact that Λ has to be positive, let the following loading criterion for the plastic stretching be assumed:

$$\left.\begin{array}{l}\mathbf{D}^{p}\neq\mathbf{0}:\ \Lambda>0,\\ \mathbf{D}^{p}=\mathbf{0}:\ \Lambda\leq 0.\end{array}\right\} \tag{26}$$

It should be noted that the constitutive equation formulated in the foregoing reduces to the time-independent subloading surface model when $\|\mathbf{D}\|\to 0$ and $\mathbf{D}^{c}-\mathbf{0}$. Here, note that time-independent elastoplastic deformation would hold approximately in the moderate rate of deformation for which the function U_D in the plastic modulus and the creep stretching are negligible.

Material Functions for Soils

First, let the material functions in the subloading surface model formulated in the preceding section be given for soils, whilst the ones involved in the time-independent model are given in the previous articles (Hashiguchi 1994; Hashiguchi and Chen 1998).

Let the stress function $f(\boldsymbol{\sigma})$ in the subloading surface (7) be given for soils as

$$f(\mathbf{S}) = p(1 + \chi^2) \tag{27}$$

where

$$p \equiv -\frac{1}{3}\mathrm{tr}\mathbf{S}\ ,\quad \mathbf{S}^* \equiv \mathbf{S} + p\mathbf{I} \tag{28}$$

$$\mathbf{H} \equiv \mathbf{Q} - \boldsymbol{\beta},\quad \mathbf{Q} \equiv \frac{\mathbf{S}^*}{p} \tag{29}$$

$$\chi \equiv \frac{\|\mathbf{H}\|}{m} \tag{30}$$

$$m = \frac{2\sqrt{6}\sin\phi}{3 - \sin\phi\sin 3\theta_\eta} \tag{31}$$

$$\sin 3\theta_\eta \equiv -\sqrt{6}\frac{\mathrm{tr}\mathbf{H}^3}{\|\mathbf{H}\|^3} \tag{32}$$

where $\mathbf{I}$ is the identity tensor and ϕ is the material constant. The tensor $\boldsymbol{\beta}$ describes the inherent anisotropy by letting the normal-yield and the subloading surfaces rotate around the origin of stress space (Sekiguchi and Ohta 1977), whilst the induced anisotropy could be described by formulating the evolution rule of $\boldsymbol{\beta}$ (cf. Hashiguchi 1994; Hashiguchi and Chen 1998). For $\boldsymbol{\beta} = \mathbf{0}$ (isotropy) the meridian section of the normal-yield and the subloading surfaces for $\theta_\eta = $ const. are half-ellipsoids whose long axes coincide with the hydrostatic axis in the stress space. The equation $\chi = 1$, i.e. $\|\mathbf{H}\| = m$ with $\boldsymbol{\beta} = \mathbf{0}$ and Eq. (31) coincides with the Coulomb-Mohr failure criterion in the axisymmetric stress state, i.e. $\|\mathbf{S}^*\|/p = 2\sqrt{6}\sin\phi/(3 \pm \sin\phi)$ (+: extension ($\theta_\eta = -\pi/6$), −: compression ($\theta_\eta = \pi/6$)). The normal-yield and the subloading surfaces described by Eqs. (5), (7) and (27) are illustrated in Fig. 3 for the axisymmetric stress state in the (p, q) plane, where

$$q = \sigma_a - \sigma_l \tag{33}$$

where σ_a and σ_l denoting the axial and the lateral stress, respectively, and β_a being the axial component of $\boldsymbol{\beta}$.

The isotropic hardening/softening function is given as

$$F = F_0 \exp\left(\frac{H}{\rho - \gamma}\right) \tag{34}$$

where F_0 is the initial value of F. ρ and γ are the slopes of normal-consolidation curve and the swelling curve, respectively, in the space (ln p, ln v) (p: pressure, v: volume). The evolution rule of the isotropic hardening/softening variable H is given as

$$\dot{H}^p = -D_v^p \equiv -\mathrm{tr}\mathbf{D}^p,\quad \dot{H}^e = -D_v^e \equiv -\mathrm{tr}\mathbf{D}^e \tag{35}$$

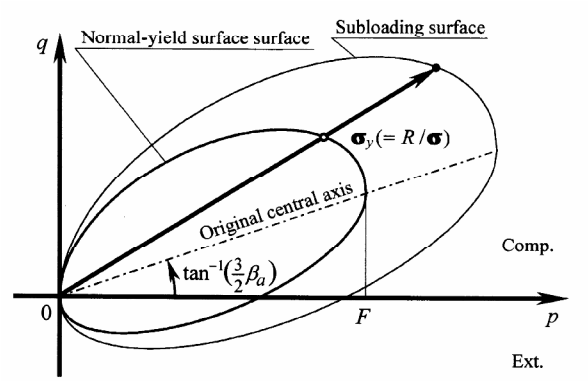

Fig. 3 Normal-yield and subloading surfaces of soils in the (p, q) plane illustrated for the state of stress over the normal-yield surface R>1 under the axisymmetric stress state

The elastic bulk modulus K in Eq. (3) is given as

$$K=\frac{p}{\gamma} \tag{36}$$

Equations. (34) and (36) are obtained from the ln v-ln p linear relation (Hashiguchi 1974), whilst the V-ln p linear relation (V ($\equiv 1+e$, e: void ratio): specific volume) adopted widely in constitutive equations of soils has physically unacceptable characteristics, as has been reviewed in detail by Hashiguchi (1995):

i) The specific volume V is predicted to be negative in high pressure p. This defect was indicated first by Butterfield (1979).

ii) The elastic bulk modulus becomes the larger value at the looser state.

iii) The elastic bulk modulus depends on the initial volume V_0, although the properties of the real material are to be independent of the initial state.

iv) The application has to be limited to the description of infinitesimal deformation.

The elastic shear modulus G is given by $G = (3/2)K(1 - 2\nu)/(1 + \nu)$ with the elastic bulk modulus K in Eq. (36) and the Poisson's ratio ν as the material constant, whilst the pertinent elastic constitutive equation of soils is proposed recently by Hashiguchi and Collins (2001).

Hashiguchi and Okayasu (2000) formulated the following equation for the creep stretching so as to describe not only the secondary consolidation effect but also the creep relaxation effect with respect to deviatoric stress state based on the empirical observations (cf. e.g. Murayama et al. 1970; Lacerda and Houston 1973), i.e.

$$\mathbf{T}=\mathbf{D}^c=D_{v0}^c\exp\left\{\frac{H}{\alpha}+\xi\left(R-\frac{F_0}{F}\right)\right\}\frac{\mathbf{N}^c}{\mathrm{tr}\mathbf{N}^c} \tag{37}$$

Let Eq. (37) be extended by considering the fact that the creep effect is suppressed at near the isotropic stress state and is induced remarkably with the increase of χ as follows:

$$\mathbf{T}=D_{v0}^c\exp\left\{\frac{-H}{\alpha}+\xi_1\left(R-1\right)+\xi_2\chi\right\}\frac{\mathbf{N}^c}{\mathrm{tr}\mathbf{N}^c} \tag{38}$$

where $\mathbf{N}^c$ is the normalized outward-normal of the creep potential surface, i.e.

$$\mathbf{N}^c \equiv \frac{\partial f^c(\boldsymbol{\sigma})}{\partial \boldsymbol{\sigma}} \Big/ \left\| \frac{\partial f^c(\boldsymbol{\sigma})}{\partial \boldsymbol{\sigma}} \right\| \tag{39}$$

$$f^c(\boldsymbol{\sigma}) = p'(1 + \chi^{c2}) \tag{40}$$

$$\chi^c \equiv \frac{\|\boldsymbol{\eta}\|}{m^c} \tag{41}$$

$$m^c \equiv \frac{\exp\{a(\chi - 1)\}}{R^b} m \tag{42}$$

ξ, ξ_1, ξ_2, a and b are material constants. The meridian section of the creep potential surface for θ_η = const. is the ellipsoid passing through the origin of stress space and the current stress point. The variation of the creep potential surface with the values of χ and R is illustrated in Fig. 4.

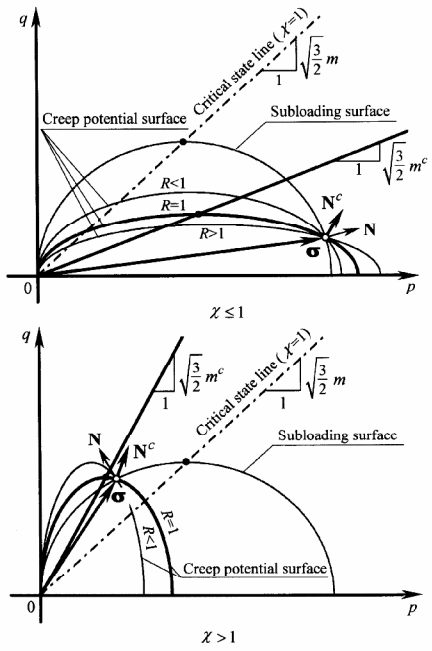

Fig. 4 Variation of the creep potential surface with the values of χ and R

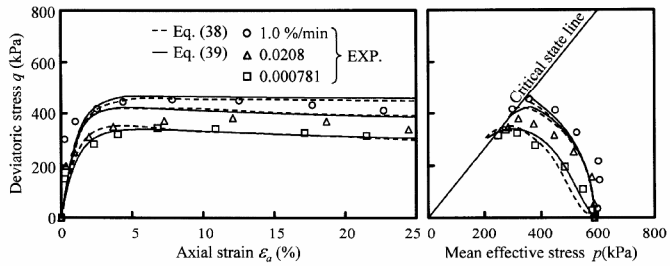

Fig. 5 Undrained triaxial compression with various strain rates (test data after Adachi et al. 1985)

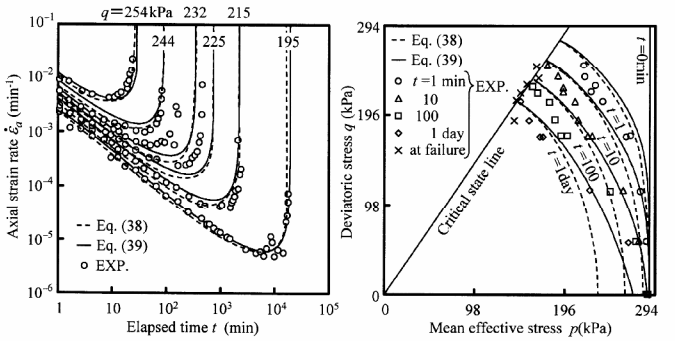

Fig. 6 Undrained triaxial creep-rupture at various deviatoric stress levels (test data after Murayama et al. 1970)

Mechanical Responses under Undrained Triaxial Compression

The mechanical responses of the model are examined for the several series of test data for clays under undrained triaxial compression in this section.

First, the comparison of the present model with Adachi *et al.*'s (1985) test data on undisturbed samples of Osaka alluvial clay subjected to the various strain rates is shown in

Fig. 5. The material constants and the initial values are selected as follows:

$$\phi = 36.0^\circ,\ \rho = 0.149,\ \gamma = 0.046,\ \nu = 0.3,\ u = 10.0,$$
$$F_0 = 294.0\ \text{kPa},\ \boldsymbol{\sigma}_0 = -294.0\mathbf{I}\ \text{kPa};$$
$$\zeta = 250.0\ \text{min},\ \alpha = 0.005,\ \xi_1 = 8.0,\ \xi_2 = 3.3,\ a = 0.6,\ b = 0.1$$
$$D_{v0}^c = -0.000008\ \text{min}^{-1},$$

where $\boldsymbol{\sigma}_0$ is the initial value of $\boldsymbol{\sigma}$. The unrealistically large isotropic creep relaxation at the low stress ratio in the p-q space is predicted by Eq. (37). On the other hand, it is suppressed realistically by the proposed creep stretching equation (38).

Figure 6 shows the comparison of the present model with Murayama *et al.*'s (1970) test data on undisturbed samples of Umeda clay subjected to the creep rupture under various values of q in which the relationships of the axial strain rate $\dot{\varepsilon}_a$ versus the time t elapsed after the stress was kept constant are shown. The material constants and the initial values are selected as follows:

$$\phi = 36.0^\circ,\ \rho = 0.149,\ \gamma = 0.046,\ \nu = 0.3,\ u = 10.0,$$
$$F_0 = 294.0\ \text{kPa},\ \boldsymbol{\sigma}_0 = -294.0\mathbf{I}\ \text{kPa};$$
$$\zeta = 100.0\ \text{min},\ \alpha = 0.003,\ \xi_1 = 8.0,\ \xi_2 = 12.0,\ a = 0.4,\ b = 0.1$$
$$D_{v0}^c = -0.000005\ \text{min}^{-1}$$

Fairly good prediction is observed for the relationship between $\log\dot{\varepsilon}_a$ and $\log t$. The unrealistically large isotropic creep relaxation at the low stress ratio in the p-q space is predicted by the creep stretching equation (37). The defect is obviously improved by the creep stretching given in Eq. (38).

FINITE ELEMENT ANALYSIS

Rate Expression of Virtual Work Principle

The rate expression of virtual work principle based on the finite deformation theory with the updated-Lagrangian scheme (e.g. Yatomi et al. 1989; Asaoka et al. 1994, 1995 and 1997) is given by

$$\begin{aligned}\int_v [\boldsymbol{\sigma}\ \delta\mathbf{D} + \{(\text{tr}\mathbf{D})\boldsymbol{\sigma} - \boldsymbol{\sigma}\mathbf{L}^T\} : \mathbb{I}\ \mathbf{L}]\text{d}v - \int_v \dot{p}_w(\text{tr}\delta\mathbf{D})\text{d}v \\ - \int_v \rho_w(\text{tr}\mathbf{D})\mathbf{b}\cdot\delta\mathbf{v}\text{d}v = \int_s \dot{\boldsymbol{\pi}}\cdot\delta\mathbf{v}\text{d}s\end{aligned} \tag{43}$$

with the nominal traction force rate in the current configuration as

$$\dot{\boldsymbol{\pi}} = \dot{\bar{\mathbf{t}}} + (\text{tr}\mathbf{D} - \mathbf{n}\cdot\mathbf{D}\mathbf{n})\bar{\mathbf{t}} \tag{44}$$

where $\mathbf{n}$ is the unit outward-normal to the boundary surface. ρ_w is unit mass of water. $\mathbf{b}$ is the body force per unit mass. The letters v and s denote the volume and the area of the body in the current configuration, respectively. $\delta(\ )$ stands for the virtual increment. $\bar{\mathbf{t}} = \boldsymbol{\sigma}\mathbf{n}$ is the traction force of the total Cauchy stress, which is obtained by

$$\boldsymbol{\sigma} = \boldsymbol{\sigma}' - p_w \mathbf{I} \tag{45}$$

p_w is the pore-water pressure (compression is a positive).

The *Zaremba*-Jaumann rate is used for the corotational rate of the effective stress $\boldsymbol{\sigma}'$:

$$\boldsymbol{\sigma}' = \boldsymbol{\sigma}'^{\circ} - \boldsymbol{W}\boldsymbol{\sigma}' + \boldsymbol{\sigma}'\boldsymbol{W} \tag{46}$$

where **W** is the continuum spin (screw-symmetric part of velocity gradient).

Continuity Condition of Soil-Water System

For solving the additional field variable $\dot{p}_w$ in Eq. (43) the following equation should be introduced simultaneously:

$$\left(\int_v \mathrm{d}v\right)^{\bullet} = \int_v \mathrm{tr}\mathbf{D}\,\mathrm{d}v = -\int_s \mathbf{v}\cdot\mathbf{n}\,\mathrm{d}s \tag{47}$$

where **v** is the discharge velocity of pore water. Eq. (47) is expanded based on the *Darcy's law* into the form:

$$\mathbf{v} = -k\frac{\partial \mathbf{h}}{\partial \mathbf{x}} = -k\frac{\partial}{\partial \mathbf{x}}\left(\mathbf{z} + \frac{p_w \mathbf{I}}{\gamma_w}\right) \tag{48}$$

where k is the coefficient of permeability. **h**, **z** and γ_w are the total head, the elevation head and the unit weight of water, respectively.

Soil-Water Coupled Stiffness Equation

The elastoplastic constitutive relation (25) is decomposed into the parts due to the stretching term and the creep term, i.e.

$$\boldsymbol{\sigma}^{\circ} = \mathbf{E}\left\{\mathbf{I} - \frac{\mathbf{N}\otimes\mathbf{NE}}{M_p^t + \mathrm{tr}(\mathbf{NEN})}\right\}\mathbf{D} + \frac{\frac{F'}{F}\dot{H}^c\,\mathrm{tr}(\mathbf{N}\boldsymbol{\sigma}') + \mathrm{tr}(\mathbf{NE}\boldsymbol{\tau})}{M_p^t + \mathrm{tr}(\mathbf{NEN})}\mathbf{EN} - \mathbf{E}\boldsymbol{\tau}. \tag{49}$$

The global stiffness equation for the soil-water system is given from Eqs. (43)-(49) as follows:

$$\begin{bmatrix} \mathrm{K} & -\mathrm{B}_{\mathrm{v}}^T \\ -\mathrm{B}_{\mathrm{v}} & \theta\alpha \end{bmatrix}\begin{Bmatrix} \Delta\mathbf{v}^n \\ \mathbf{p}_w|_{t+\Delta t} \end{Bmatrix} = \begin{Bmatrix} \Delta\mathbf{f}^n - \Delta\mathbf{f}_c^n \\ \mathbf{0} \end{Bmatrix} - \begin{Bmatrix} \mathrm{B}_{\mathrm{v}}^T\mathbf{p}_w|_t \\ (1-\theta)\alpha\mathbf{p}_w|_t \end{Bmatrix} - \begin{Bmatrix} \mathbf{0} \\ \alpha(\theta\mathbf{z}|_{t+\Delta t} + (1-\theta)\mathbf{z}|_t) \end{Bmatrix} \tag{50}$$

where the stiffness matrix [K] in Eq. (50) involves the first term in Eq. (49) and then $\Delta\mathbf{f}_c^n$ is assembled by the virtual force increment due to the second and third terms in Eq. (49). $\Delta\mathbf{f}^n$ is the nodal force increment. [Bv] and [$\theta\alpha$] are the transformation matrix of the nodal displacement increment to the volumetric strain increment and the stiffness matrix of the pore water. t and Δt indicate time and time increment. The FEM program is developed based on the soil-water coupled formulation of Akai and Tamura (1978), the finite deformation theory

of Yatomi et al. (1989) and their unification of Asaoka et al. (1994, 1995 and 1997).

In addition, the stiffness equation (50) is rate-nonlinear since the plastic stretching includes the magnitude of stretching, i.e. $\|\mathbf{D}\|$ and further the elevation head depends upon the change of soil skeleton. Therefore, Eq. (50) has to be solved by the iterative calculation under the boundary conditions in general.

ONE-DIMENSIONAL CONSOLIDATION

The performance of the present FEM program is evaluated by the simulation of the one-dimensional consolidation phenomena.

Influence of Stress Rate

The stress controlled consolidation phenomena for various stress rates (high: 1×10^{-3}, middle: 1×10^{-4}, low: 1×10^{-5} kPa/min) are compared, which are simulated by the FEM program based on the time-independent and the time-dependent subloading surface models. The specimen is descretized into 42 nodes and 20 elements using the 4-nodes isoparametric quadrilateral element as shown in Fig. 7. The bottom and both side-boundaries of the specimen are given by the impermeable boundaries whilst the top of the specimen is the permeable boundary. The vertical stress is continuously increased up to −100 kPa. The specimen is left during one year in order to observe the aging effect under the constant vertical stress condition and then the vertical stress is increased continuously. The material constants and the initial values are selected as follows:

$$\phi = 30.0^\circ,\ \rho = 0.08,\ \gamma = 0.01,\ \nu = 0.3,\ u = 100.0,$$
$$F_0 = 100.0\ \text{kPa},\ \boldsymbol{\sigma}_0 = -10.0\mathbf{I}\ \text{kPa};$$
$$\zeta = 200.0\ \text{min},\ \alpha = 0.003,\ \xi_1 = 5.0,\ \xi_2 = 5.0,\ a = 0.1,\ b = 0.1,$$
$$D_{v0}^{c} = -0.00008\ \text{min}^{-1};$$
$$k = 6\times10^{-8}\ \text{m/min},\ \gamma_w = 9.8\ \text{kN/m}^3.$$

Here, note that the time-dependent constitutive equation is reduced to the time-independent (elastoplastic) one if the material constant ζ and the initial value D_{v0}^{c} are taken to be zero. The third term in Eq. (43) and the elevation head z are not considered thought the simulations since the specimen is small.

The vertical stress-volumetric strain curves and the elapsed time-volumetric strain curves at the constant stress state for the various stress rates are shown in Fig. 8. In the result of the high rate loading simulated by the FEM program with the time-independent subloading surface model the volumetric compression due to the pore water pressure dissipation is observed at the constant stress state as shown in the left of Fig. 8b. On the other hand, the volumetric compression is not observed at constant stress state since the pore water pressure dose not grow under the middle and low rate loading conditions. Further, the coupled consolidation due to the pore water dissipation and the creep effect, called the *delayed consolidation* by Bjerrum (1967), is predicted at the high rate loading by the FEM program with the time-dependent subloading surface model as shown in the right of Fig. 8b. The purely delayed consolidation is described in the middle and low rate loadings. The relation of normal-yield ratio versus vertical stress in the reference element for the middle rate loading is illustrated in Fig. 9. The creep deformation is predicted not only in the normal-yield but also in the sub-yield states whilst it cannot be predicted by the FEM program based on the models

assuming the purely elastic domain inside the yield surface, e.g. the over-stress model and the non-stationary flow surface model.

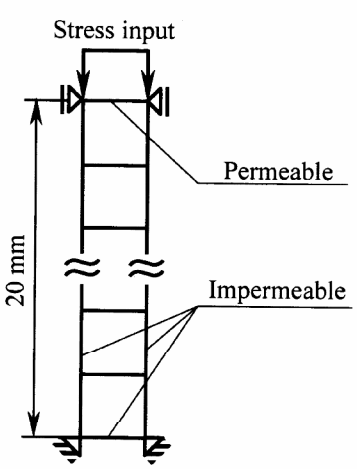

Fig. 7 FE mesh and boundary conditions for one-dimensional consolidation test

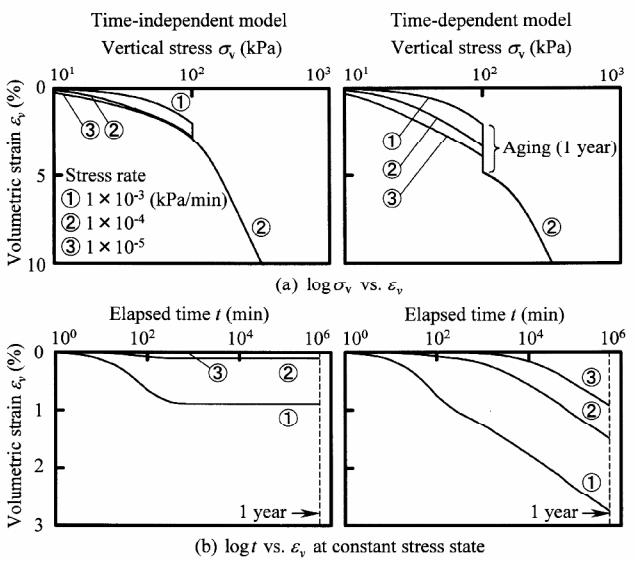

Fig. 8 Comparison of consolidation curves for various stress rates calculated by FEM program with time-independent and time-dependent subloading surface models

Influence of Specimen Thickness

The influence of the specimen thickness is examined on the elapsed time-volumetric strain relation. The specimen thickness is selected as 10 (22 nodes, 10 elements), 20 (42 nodes, 20 elements) and 60 (122 nodes, 60 elements) mm. In all simulations the vertical stress −100 kPa is applied to the top of the specimen instantaneously realizing the perfectly undrained condition and then the specimen is left during 1×10^5 min (about 70 days) under the partially drained condition.

The variations of the volumetric strain-elapsed time relations for three sizes of the specimen thickness are depicted in Fig. 10, which are calculated by the FEM program with the time-independent and the time-dependent subloading surface models. All consolidation curves analyzed by the FEM program with the time-independent subloading surface model coincide with each other after the pore water pressure is dissipated. Thus, the secondary consolidation cannot be observed without the consideration of the time-dependency of material itself. On the other hand, the secondary consolidation is described realistically by the FEM program with the time-dependent subloading surface model. Further, the volumetric strains do not coincide even when the pore water pressure is dissipated since the quantity of the consolidation induced by the creep effect increases with time. Often the consolidation phenomenon is interpreted separating into the primary (pore water pressure dissipation) and secondary (creep effect) consolidation but it should be considered as their coupled phenomenon in general. The FEM program with the time-dependent subloading surface model could predict the consolidation behavior pertinently.

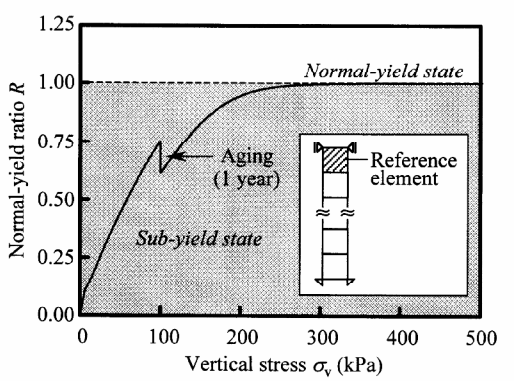

Fig. 9 Relation between normal-yield ratio and vertical stress for middle stress rate

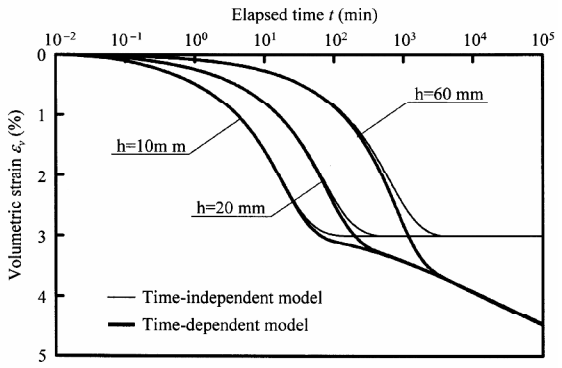

Fig. 10 Elapsed time-volumetric strain relation for three sizes of specimen thickness simulated by the FEM program with time-independent and time-dependent subloading surface models

CONCLUDING REMARKS

In this article, the creep stretching proposed by Hashiguchi and Okayasu (2000) is extended so as to suppress the isotropic stress relaxation at the low stress ratio and inversely induce a more remarkable relaxation at the high stress ratio. The FEM program based on the time-dependent subloading surface model is developed in order to analyze the boundary value problem with the time-dependent deformation behavior of soil structures. The FEM program was verified to describe pertinently the consolidation behavior due to not only the pore water pressure dissipation but also the creep in the one-dimensional consolidation.

REFERENCES

Adachi, T., Mimura, M. and Oka, F. (1985). Descriptive accuracy of several existing constitutive models for normally consolidated clays. Proc. 5th Int. Conf. Numer. Meth. Geomech., Nagoya: 259-266.

Adachi, T. and Oka, F. (1982). Constitutive equations for normally consolidated clay based on elasto-viscoplasticity. Soils and Foundations. 22(4): 57-70.

Adachi, T. and Okano, M. (1974). A constitutive equation for normally consolidated clays. Soils and Foundations. 14(4): 55-73.

Al-Shamrani, M. A. and Sture, S. (1998). A time-dependent bounding surface model for anisotropic cohesive soils. Soils and Foundations. 38(1): 61-76.

Akai and Tamura (1978). Numerical analysis of multidimensional consolidation accompanied with elasto-plastic constitutive equation. Proc. JSCE. 269: 95-104 (in janaese).

Asaoka, A., Nakano, M. and Noda, T. (1994). Soil-water coupled behavior of saturated clay near/at critical state. Soils and Foundations. 34(1): 91-105.

Asaoka, A., Nakano, M. and Noda, T. (1995). Imperfection sensitive bifurcation of Cam-Clay under plane strain compression with undrained boundaries. Soils and Foundations. 35(1): 83-100.

Asaoka, A., Noda, T. and Fernando, G. S. K. (1997). Effects of changes in geometry on the linear elastic consolidation deformation. Soils and Foundations. 37(1): 29-39.

Bjerrum, L. (1967). Engineering geology of Norwegian normally-consolidated marine clays as related to settlements of building. Geotechnique. 17: 81-118.

Butterfield, R. (1979). Elastic-plastic deformation at finite strain. Geotecnique. 29: 469-480.

Dafalias, Y. F. (1982). Bounding surface elastoplasticity-viscoplasticity for particulate cohesive media. Proc. IUTAM Symp. Deformation and Failure of Granular Materials. Delft: 97-107.

Dafalias, Y. F. (1985). The plastic spin. J. Appl. Mech. (ASME). 52(4): 865-871.

Drucker, D. C. (1988). Conventional and unconventional plastic response and representation. Appl. Mech. Rev. (ASME), 41(4): 151-167.

Hashiguchi, K. (1974). Isotropic hardening theory of granular media. Proc. JSCE. 227: 45-60

Hashiguchi, K. (1980). Constitutive equations of elastoplastic materials with elastic-plastic transition. J. Appl. Mech. (ASME). 47(2): 266-272.

Hashiguchi, K. (1989). Subloading surface model in unconventional plasticity. Int. J. Solids Struct.. 25(8): 917-945.

Hashiguchi, K. (1994). Subloading surface model with rotational hardening. Proc. Int. Conf. Compt. Methods in Struct. & Geotech. Eng.. Hong Kong: 807-812.

Hashiguchi, K. (1995). On the linear relations of V-lnp and lnv-lnp for isotropic consolidation of soils. Int. J. Numer. Anal. Meth. Geomech.. 19(3): 367-376.

Hashiguchi, K. and Chen, Z.-P. (1998). Elastoplastic constitutive equations of soils with the subloading surface and the rotational hardening. Int. J. Numer. Anal. Meth. Geomech.. 22(2): 197-227.

Hashiguchi, K. and Collins, I. F. (2001). Stress rate-elastic stretching relations in elastoplastic constitutive equations. Soils and Foundations. 41(2), 77-87.

Hashiguchi, K. and Okayasu, T. (2000). Time-dependent elastoplastic constitutive equation based on the subloading surface model and its application to soils. Soils and Foundations. 40(4): 19-36.

Hashiguchi, K. and Ueno, M. (1977). Elastoplastic constitutive laws of granular materials. Constitutive Equations of Soils (Proc. 9th ICFSME, Spec. Session 9), Tokyo, JSSMFE. Tokyo: 73-82.

Kaliakin, V. N. and Dafalias, Y. F. (1990a). Theoretical aspects of the elastoplastic-viscoplastic bounding surface model for cohesive soils. Soils and Foundations. 30(3): 11-24.

Kaliakin, V. N. and Dafalias, Y. F. (1990b). Verification of the elastoplastic-viscoplastic bounding surface model for cohesive soils. Soils and Foundations. 30(3): 25-36.

Lacerda, W. A. and Houston, W. N. (1973). Stress relaxation in soils. Proc. 8th ICSFME. Moscow: 221-227.

Liang, R. Y. and Ma, F. (1992). A unified elasto-viscoplasticity model for clays, Part I: Theory. Compt. Geotech.. 13(2): 71-87.

Matsui, T. and Abe, N. (1985). Elasto-viscoplastic constitutive equation of normally consolidated clays based on flow surface theory. Proc. 5th Int. Conf. Numer. Meth. Geotech.. Nagoya. 1: 407-413.

Murayama, S. Kurihara, N. and Sekiguchi, H. (1970). On creep rupture of normally consolidated clays. Annuals, Disaster Prevention Research Institute. Kyoto Univ.: 13(B): 525-541 (in Japanese).

Nova, R. (1982). A viscoplastic constitutive model for normally consolidated clay. Proc. IUTAM Symposium on Deformation and Failure of Granular Materials. Delft: 287- 295.

Olszak, W. and Perzyna, P. (1966). The constitutive equations of the flow theory for a non-stationary yield condition. Proc. 11th Int. Congress of Applied Mechanics: 545-553.

Olszak, W. and Perzyna, P. (1970). Stationary and nonstationary viscoplasticity. Inelastic Behavior of Solids. McGraw-Hill: 53-75.

Perzyna, P. (1963a). The constitutive equations for rate sensitive plastic materials. Quart. Appl. Math.. 20(4): 321-332.

Perzyna, P. (1963b). The constitutive equations for workhardening and rate sensitive plastic materials. Proc. Vibration Problems. Warsaw. 3(3): 281-290.

Perzyna, P. (1966). Fundamental problems in viscoplasticity. Advances in Applied Mechanics. 9: 243-377.

Sekiguchi, H. (1977). Rheological characteristics of clays. Proc. 9th ICSFME. Tokyo. 1: 289-291.

Sekiguchi, H. (1984). Theory of undrained creep rupture of normally consolidated clay based on elasto-viscoplasticity. Soils and Foundations. 24(1): 129-147.

Sekiguchi, H. and Ohta, H. (1977). Induced anisotropy and its time dependence in clays. Constitutive Equations of Soils (Proc. Spec. Session 9, 9th ICSFME). Tokyo: 229-238.

Tian, W.-M., Sadd, M. H., Silva, A. J. and Veyera, G E. (1994). Modeling creep behavior of anisotropically consolidated marine clays. Proc. Compt. Meth. & Advances in Geomech.. Morgantown (West Virginia): 701-706.

Yatomi, C., Tashima, A., Iizuka, A. and Sano, I. (1989). General theory of shear bands formulation by a non-coaxial Cam-clay models. Soils and Foundations. 29(3): 41-53.

Zbib, H. M. and Aifantis, E. C. (1988). On the concept of relative and plastic spins and its implications to large deformation theories. Part I: Hypoelasticity and vertex-type plasticity. Acta Mech.. 75: 15-33.